Electronic Supplementary Information

Thermally Stimulated Cascade Reaction Polymer Membranes: A Promising Strategy for an increased Hydrogen and Propylene Purification Performance

Authors: David Meis, Silvio Neumann, Sergey Shishatskiy, Ulrike Meis, Volkan Filiz

Affiliations:

Helmholtz-Zentrum Hereon, Institute of Membrane Research, Max-Planck-Str.1, 21502 Geesthacht, Germany

*Email: volkan.filiz@hereon.de

Table of Content

Polymer Synthesis

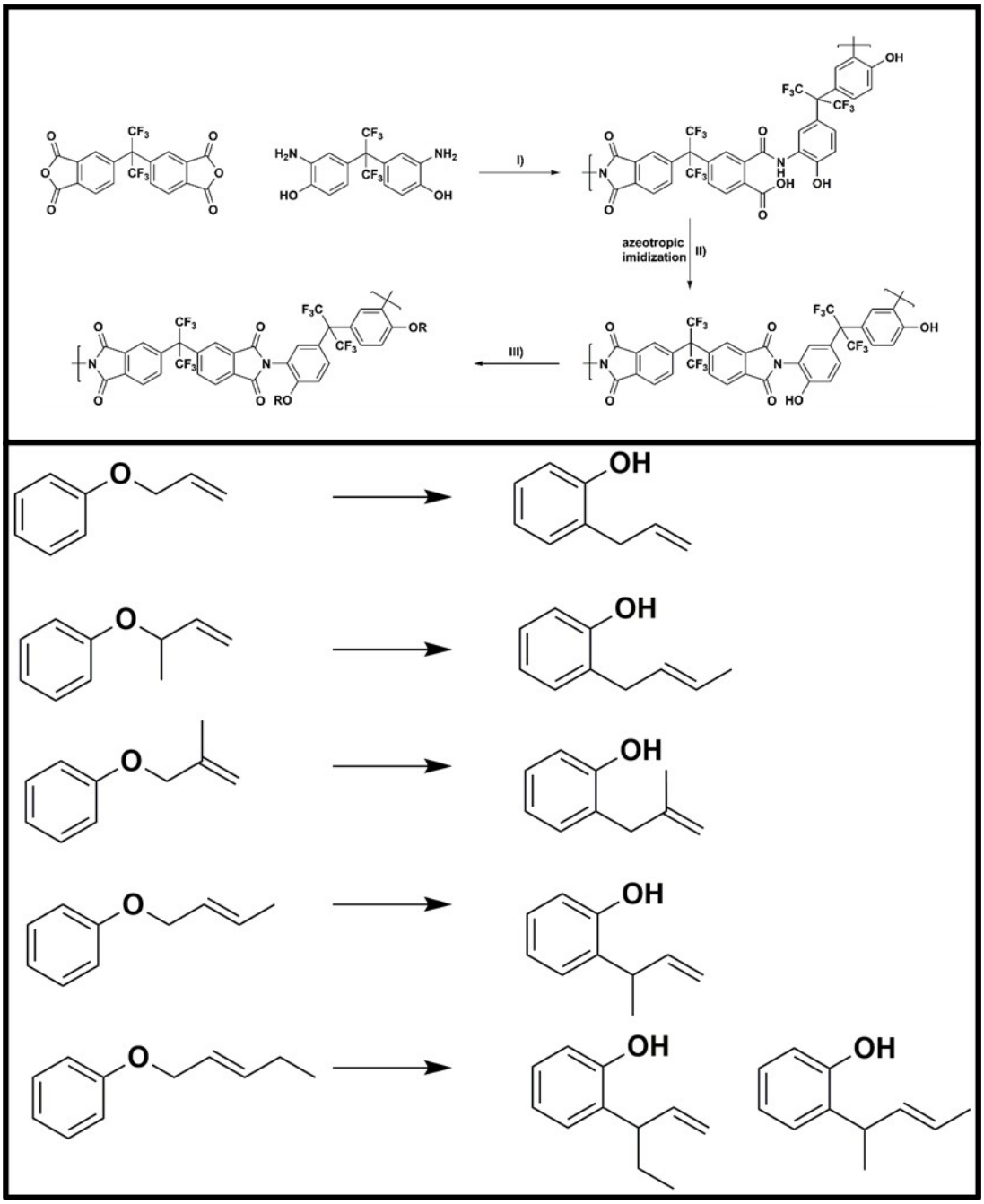

Scheme S1. Synthesis route for the polymerization, imidization and allylation. (I) Polyamic acid formation, (II) azeotropic imidization at 180 °C with *o*-xylene, (III) *ortho*-hydroxy group conversion. Overview of the formed structures after the Claisen-Rearrangement.

Polymer Characterization

Polymer characterization methods

The polymers were characterized by ^{1}H-Nuclear Magnetic Resonance (NMR) spectroscopy employing a Bruker AVIIIHD spectrometer at 500 MHz (^{1}H-NMR), with deuterated dimethyl sulfoxide (DMSO-d_6) as the solvent and lock signal. Tetramethylsilane (TMS) was used as a reference signal.

The standard-equivalent molecular weights of the functionalized polyimides was determined by gel permeation chromatography (GPC) based on standard polystyrene calibration using the PSS ReadyCal-Kits Poly(Styrene) pskitr4-12 with a molar mass range from Mp 474 - 2 520 000 Da, in dimethylacetamide (DMAc) with the addition of lithium chloride (2.12 g L^{-1}) I the eluent in each measurement. A Waters 717plus instrument equipped with PSS GRAM columns [GRAM pre-column (dimension 8 – 50 mm) and two GRAM columns of different porosity (3000 Å and 1000 Å, respectively) with dimension of 8 · 300 mm and particle size of 10 µm. The flow rate was 1,0 mL min^{-1} using a VWR-Hitachi 2130 pump, and a Shodex RI-101 differential refractive index detector was used.

Attenuated total internal reflectance - Fourier transform infrared spectroscopy (ATR-FTIR) measurements were performed using a Bruker alpha ATR in a spectral range of 400-4000 cm^{-1} with an accumulation of 32 scans and a resolution of 4 cm^{-1}.

Differential scanning calorimetry (DSC) was performed with a differential scanning calorimeter DSC1 (Mettler-Toledo) in a temperature range between 30 and 450 °C under nitrogen (60 mL min^{-1}) and at a heating rate of 5 °C min^{-1} to study the thermally induced transitions of the synthesized polyimides. Approximately 8 mg of the polymer sample were transferred into a 40 µL sealed aluminum pan with a pierced lid. For the glass transition determination, the materials were heated up to 300 °C and held for 30 min, and cooled down afterwards at a heating rate of 5 and cooling rate of 10 °C min^{-1}. The glass transition was determined during the second cycle. All measured heat flows are weight-normalized.

Thermogravimetric analysis (TGA) was performed using a TGA-DSC2 Thermogravimetric Analyzer (Mettler-Toledo) over the range of 25 to 800 °C with a heating rate of 5 °C min^{-1} in an argon atmosphere (both with a flow rate of 20 mL min^{-1}). In order to determine the CO_2 as well as other volatile products evolution during TR-process, the thermogravimetric analyzer was coupled with a FTIR spectrometer Nicolet iS50 (Thermo Scientific), which recorded in the spectral range of 400-4000 cm^{-1} with a resolution of 4 cm^{-1} and a total number of 64 scans per spectrum. The conversion of the Thermal Rearrangement process for each material after different isothermal treatments was obtained by performing TGA runs of these materials. Afterwards the mass loss of the corresponding mass loss step, in the temperature range between the determined onset- and offset-temperature, was measured. With this experimental mass loss, the conversion was calculated according to the following equation:

$$conversion\ (\%) = \frac{mass\ loss\ _{experimental}}{mass\ loss\ _{theoretical}} x100 \qquad \text{(eq. S1)}$$

The density of the membranes was determined by using a Mettler Toledo XP105 balance equipped with a density determination kit. The samples were weighed in air and isooctane according to the buoyancy method. Isooctane has been chosen as a liquid with known density since it is wetting the membrane perfectly and is not absorbing into the membrane. The density was calculated using the following equation (eq. S2)

$$\rho_{membrane} = \frac{w_{air}}{w_{air} - w_{liq}} \rho_{liq} \qquad \text{(eq. S2)}$$

with $\rho_{membrane}$ as the membrane density (g cm^{-3}), w_{air} and w_{liq} as the weight of the membrane in air and isooctane (g), and ρ_{liq} is the density of isooctane (g cm^{-3}).

Based on the density data, the fractional free volume (FFV) of the membranes before the thermal treatments was estimated according to the following equation (eq. S3)

$$V_{sp} = \frac{m}{\rho_{membrane}} \qquad \text{(eq.S3)}$$

$$FFV = \frac{V_{sp} - 1.3xV_w}{V_{sp}} \quad \text{(eq.S4)}$$

Where V_{sp} is the specific molar volume of the polymer membrane and V_w is the van der Waals molar volume according to Bondi's group contribution theory [1, 2].

X-ray diffraction measurements of the membranes were done using a Siemens D5000 diffractometer with a Cu Kα radiation with a wavelength of 0.154 nm at a step size of 0.1° min^{-1} and a step time of 4 s in the 2θ range of 2 - 50°. The average d-spacing value was calculated via Bragg's equation:

$$2d\sin\theta = n\lambda \quad \text{(eq. S5)}$$

The gas permeation properties were determined using a constant volume variable pressure method (time-lag method) realized in an in-house designed and built experimental facility [3]. The single gas permeability P of H_2, He, N_2, O_2, CH_4, CO_2, C_2C_4, C_2C_6, C_3C_6, C_3C_8 was measured at 30 °C and a feed pressure of 1000 mbar. From the linear increase of the downstream pressure rise as a function of the time (dp/dt) the permeability of each gas could be calculated with the equation:

$$P = \frac{273.15Vldp}{76T\Delta pA\ dt} \quad \text{(eq. S6)}$$

with permeability *P* (Barrer), membrane thickness *l* (cm) (see Table S1), downstream chamber volume *V* of 43.3 cm³ temperature *T* of 303 K, pressure difference *dp* (=$p_{upstream}$-$p_{downstream}$) (cm Hg) and effective membrane area *A* of 1.22cm². Based on the calculated permeability of each gas, the ideal selectivity $\alpha_{x/y}$ of each gas pair could be calculated, as shown in equation S7

$$\propto_{x/y} = \frac{P_x}{P_y} \quad \text{(eq. S7)}$$

The diffusion coefficients were obtained from these steady-state measurements by determination of the diffusional time-lag θ. The time-lag is determined by the intersection of time-axis and tangent of the steady-state range. By means of equation S8, the diffusion coefficient D was calculated:

$$\theta = \frac{l^2}{D} \qquad \text{(eq. S8)}$$

Claisen Rearrangement mechanism

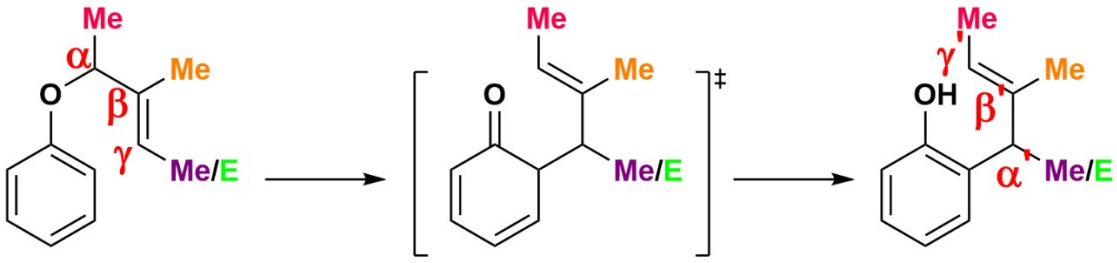

Scheme S2. Claisen Rearrangement mechanism.

Structure Characterization of annealed βMPI-1

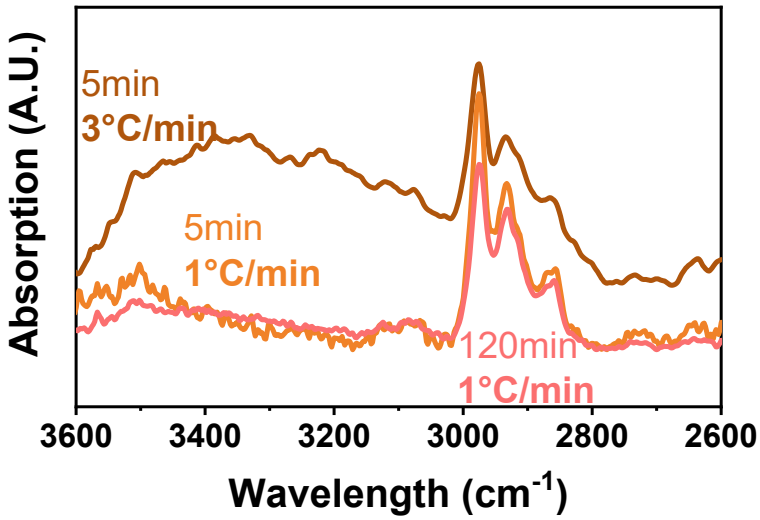

Figure S1. FT-IR spectrum of the annealed samples of MPI-1 after annealing at 300 °C with a heating rate of 3 °C/min and 1 °C/min, and a sample that was heated with a heating rate of 1 °C/min and an isothermal treatment for 2 h.

Structure Characterization of βMallyloxy-modified Backbones

βM-PI-1

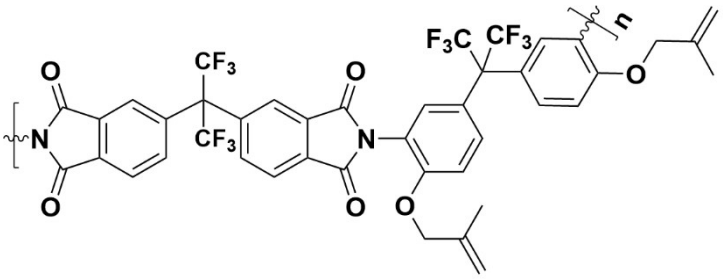

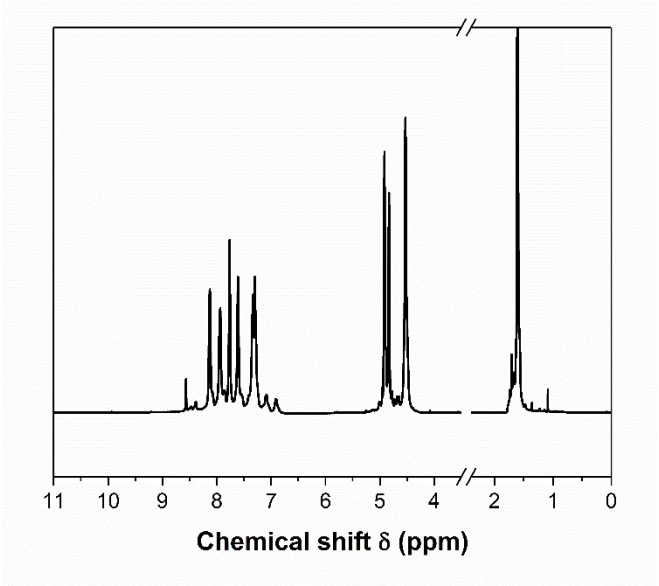

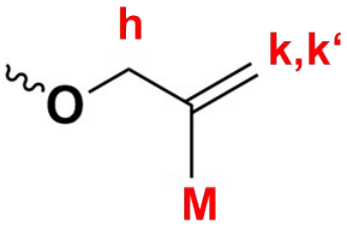

Figure S2. ^{1}H-NMR spectrum *β*M-PI.

Molecular weight: Mn (g/mol), = 2.47·10^{4}, Mw (g/mol), = 9.91·10^{4}, Đ = 4.0. IR: 3082 (w, C-H str., alkene); 2925 (w, C-H str., alkane, methyl); 2875 (w, C-H str., alkane, methylene); 1789 (s, C=O str, imide); 1725 (w, C=O str, imide); 1615 (w, C=C str., alkene); 1273,1205 (s, C-O-C str., ether). ^{1}H NMR (DMSO-d6, ppm); For specific assignments see Figure S2: 7.3-8.2 (m, 12 H, aromatic, **a-f**); 4.8-4.9 (m, 4 H, vinyl, **k,k'**); 4.5 (s, 4 H, allylic, **h**); 1.6 (s, 6 H, allylic, **M**).

βM-PI-2

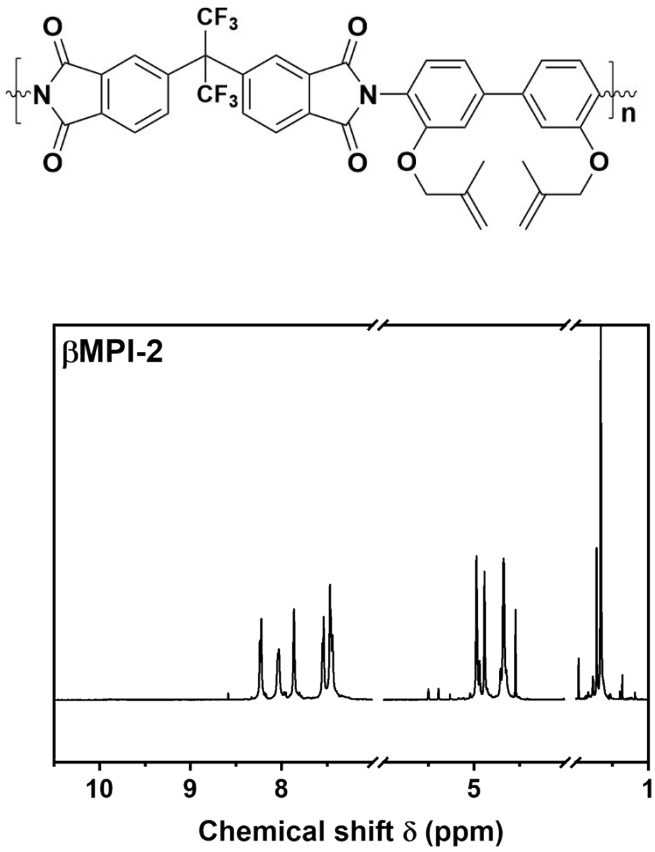

Figure S3. ^{1}H-NMR spectrum βM-PI-3.

Molecular weight: Mn (g/mol), = 2.92·10^{4}, Mw (g/mol), = 8.13·10^{4}, Đ = 2.78. ^{1}H NMR (DMSO-d6, ppm); For specific assignments see Figure S3: 7.3-8.4 (m, 12 H, aromatic); 4.9-5.1 (m, 4 H, vinyl, **k,k'**); 4.6 (s, 4 H, allylic, **h**); 1.6 (s, 6 H, allylic, **M**).

βM-PI-3

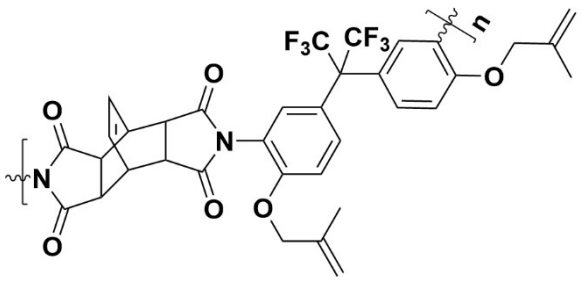

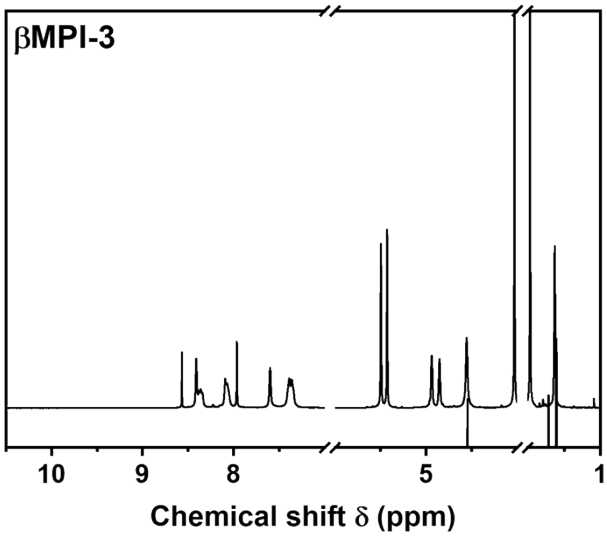

Figure S4. ^{1}H-NMR spectrum βM-PI-2.

Molecular weight: Mn (g/mol), = $1.29 \cdot 10^4$, Mw (g/mol), = $5.58 \cdot 10^4$, Đ = 4.31. ^{1}H NMR (DMSO-d6, ppm); For specific assignments see Figure S4: 7.3-8.2 (m, 6 H, aromatic); 5.4-5.6 (m, 2 H, vinyl anhydride); 4.8-4.9 (m, 4 H, vinyl, **k,k'**); 4.6 (s, 4 H, allylic, **h**); 2.0 (s, 2 H, xxxx); 1.6 (s, 6 H, allylic, **M**).

βM-PI-4

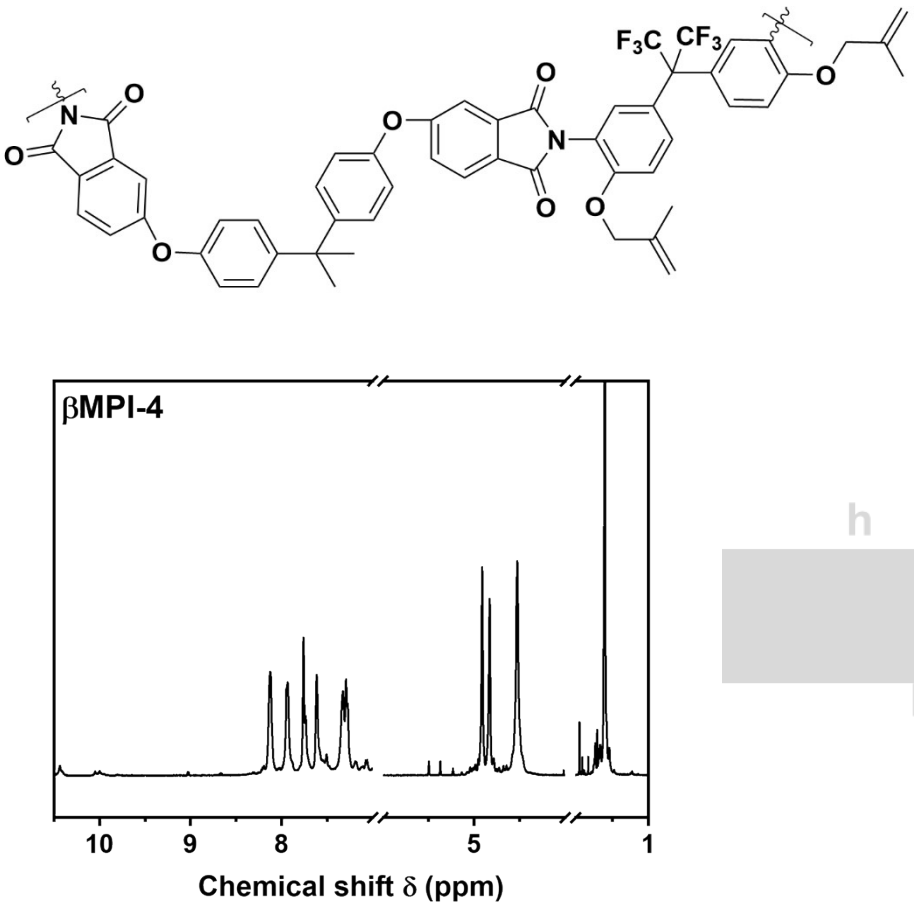

Figure S5. ^{1}H-NMR spectrum βM-PI-4.

Molecular weight: Mn (g/mol), = $3.37 \cdot 10^4$, Mw (g/mol), = $6.80 \cdot 10^4$, Đ = 2.02. ^{1}H NMR (DMSO-d6, ppm); For specific assignments see Figure S5: 7.3-8.2 (m, 20 H, aromatic); 4.8-4.9 (m, 4 H, vinyl, **k,k'**); 4.5 (s, 4 H, allylic, **h**); 1.6 (s, 6 H, allylic, **M**).

βM-PI-5

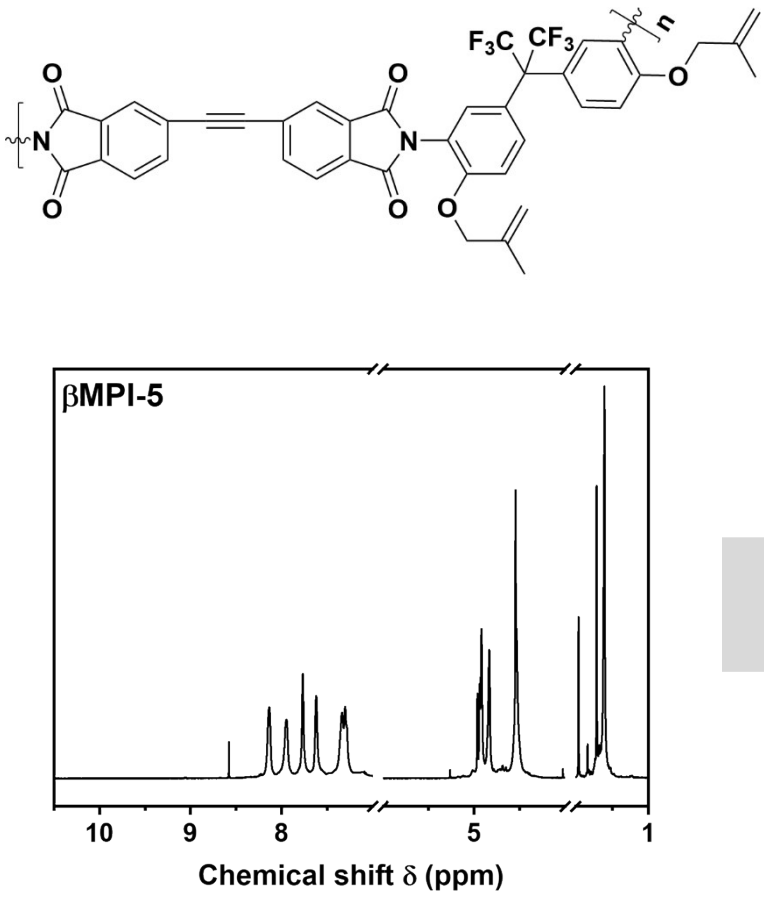

Figure S6. ^{1}H-NMR spectrum βM-PI-5.

Molecular weight: Mn (g/mol), $3.79 \cdot 10^4$, Mw (g/mol), = $16.9 \cdot 10^4$, Đ = 4.49. ^{1}H NMR (DMSO-d6, ppm); For specific assignments see Figure S6: 7.3-8.2 (m, 12 H, aromatic, **a-f**); 4.8-4.9 (m, 4 H, vinyl, **k,k'**); 4.5 (s, 4 H, allylic, **h**); 1.6 (s, 6 H, allylic, **M**).

Thermal Characterization of βMallyloxy-modified Backbones

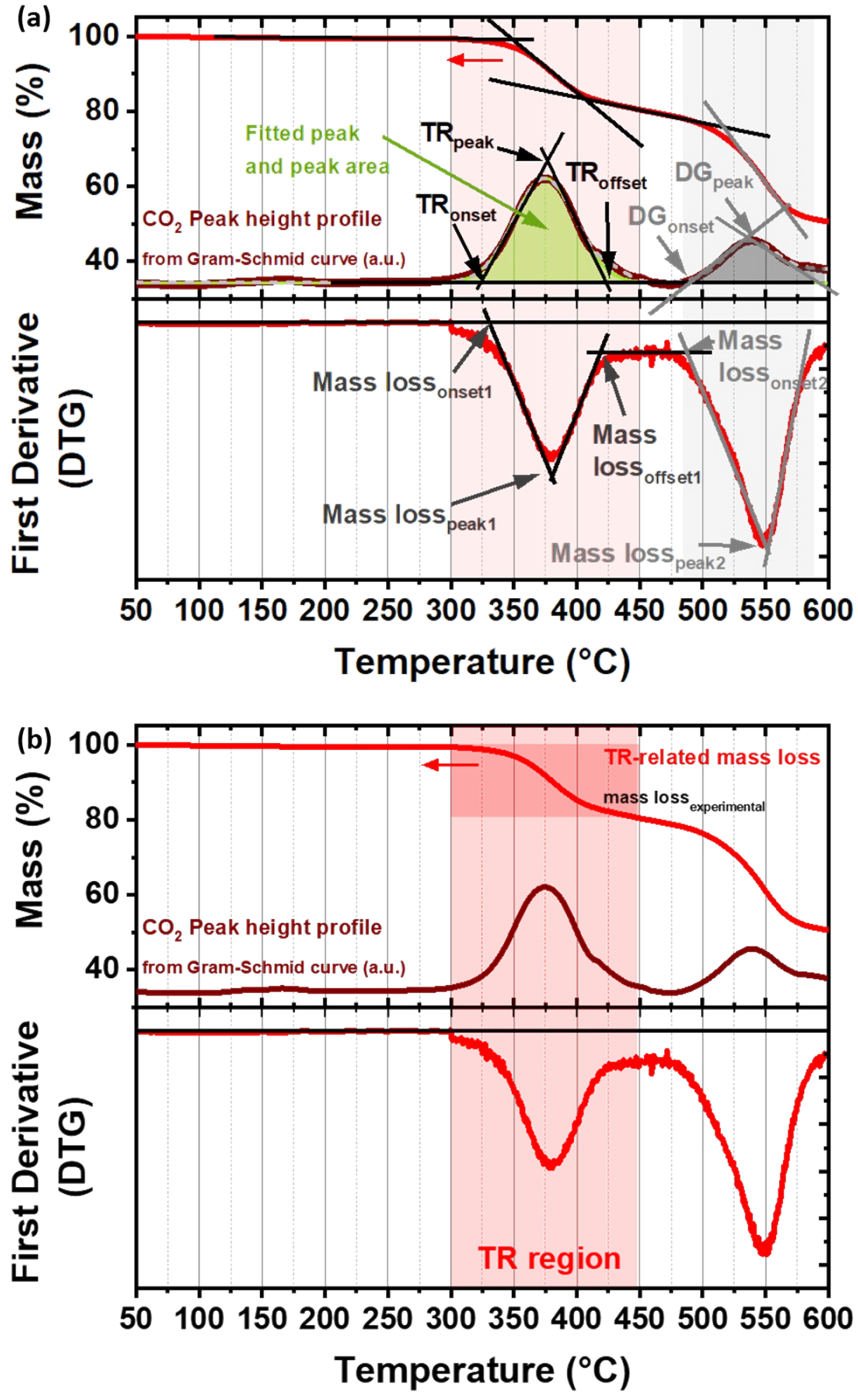

Figure S7. (a) Determination of the TR and degradation (DG) specific onset, peak and offset temperature, as well as the mass loss onset, peak and offset temperature of the first and

second mass loss corresponding process. (b) TGA-mass loss curve, its first derivative (DTG) and extracted CO_2 peak height profile, including the region of the determined experimental mass loss for the TR conversion calculation.

Residual mass loss in the TR region is divided by the theoretical mass loss of 2 molecules of CO_2 per repetition unit, as expected for a quantitative PBO conversion, yields the TR conversion.

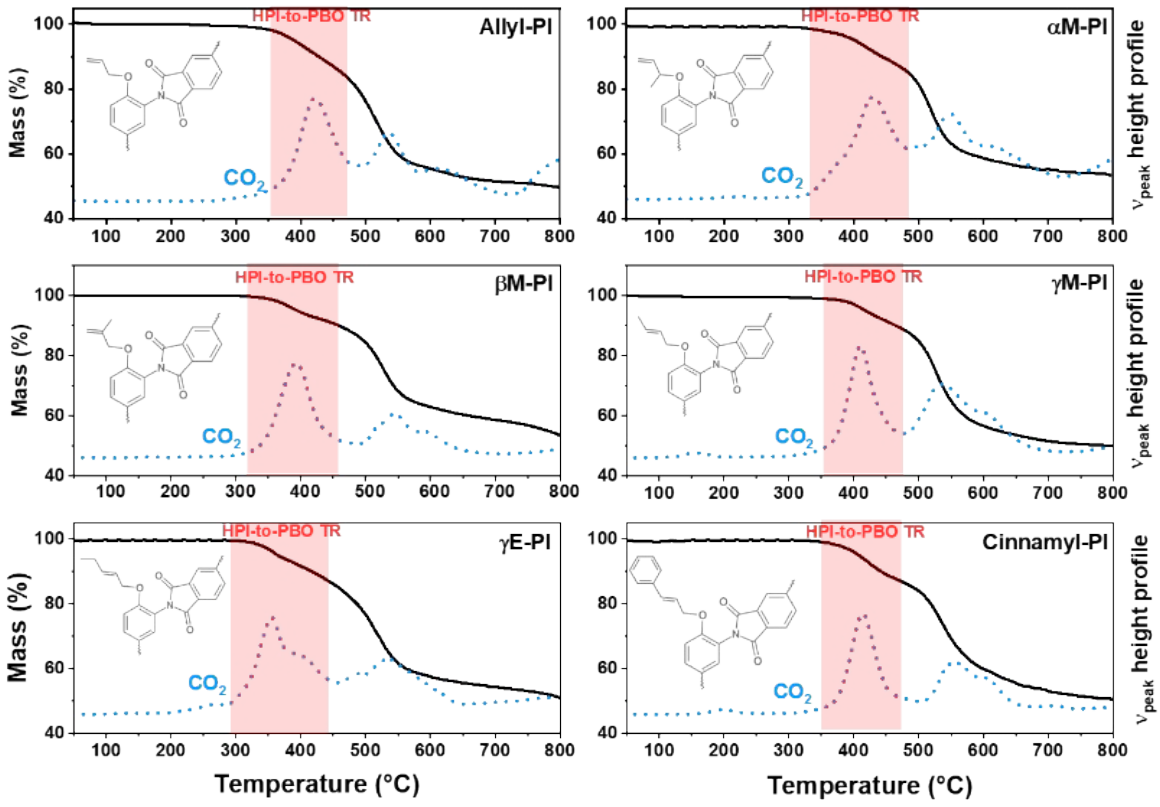

Figure S8. Mass loss curves (black) and CO_2 peak height profiles (blue) measured by DSC for all Claisen Rearrangement undergoing polymers.

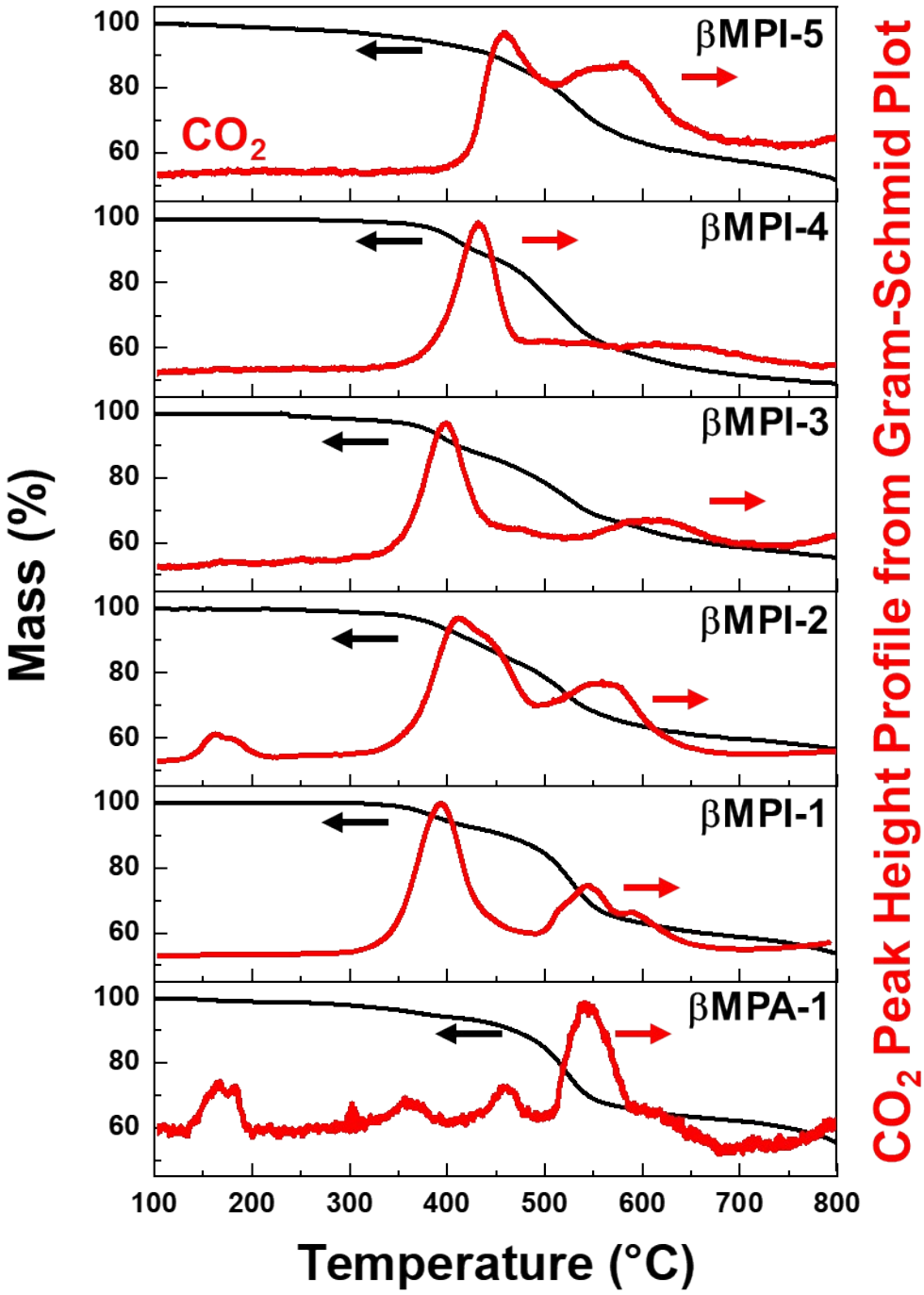

Figure S9. TGA based mass loss curves (black) and CO_2 peak height profile, determined by evolved decomposition gas analysis via FT-IR spectroscopy (red) of βMallyloxy-modified polyamide βMPA-1 and polyimide βMPI-1, -2, -3, -4, and -5.

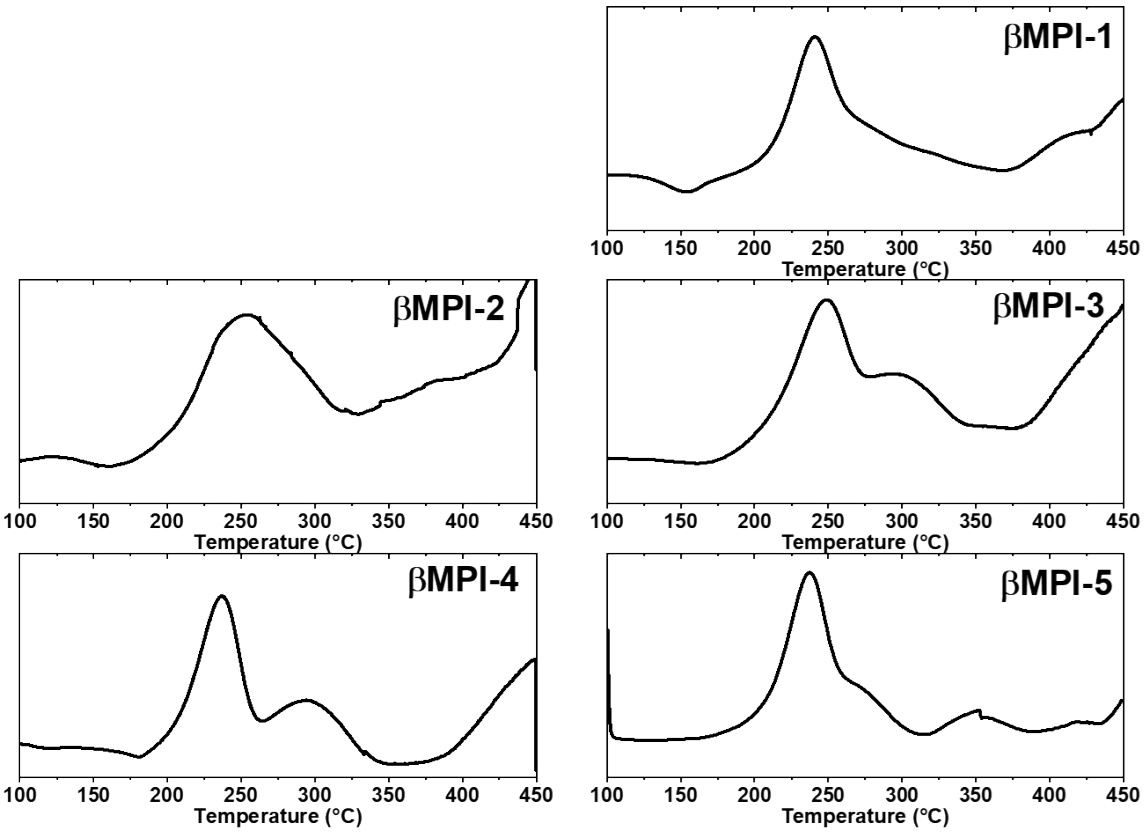

Figure S10. DSC based heat flow curves of βMallyloxy-modified polyimide βMPI-1, -2, -3, -4, and -5.

Table S1. Determined physical properties glass-transition temperature Tg, TR onset temperature TR_{on}, TR conversion TR%, density, fractional free volume FFV of Allyl-, αM-, βM-, γM- and γE-PI.

Modification	Tg (°C)	TR_{on} (°C)	TR% (%)	Density (g/cm³)	FFV (%)	ΔThickness (%)
Allyl-PI	N.A.	331		1.42±0.017	17.3	
Allyl-PI 300 °C			12.6	1.35±0.025	20.6	5.47
Allyl-PI 350 °C			48.5	1.33±0.016	20.9	7.39
Allyl-PI 400 °C			100	1.32±0.010	20.9	4.31
αM-PI	333	328		1.41±0.010	15.7	
αM-PI 300 °C			13.0	1.36±0.001	16.6	2.10
αM-PI 350 °C			62.1	1.35±0.007	18.3	2.24
αM-PI 400 °C			100	1.32±0.007	20.8	3.35
βM-PI	302	325		1.40±0.018	16.9	
βM-PI 300 °C			14.6	1.35±0.016	18.7	7.45
βM-PI 300 °C			22.2	1.34±0.022		1.75
βM-PI 350 °C			84.8	1.31±0.013	20.6	17.4
βM-PI 400 °C			100	1.31±0.013	22.3	3.00
γM-PI	289	352		1.40±0.007	15.9	
γM-PI 300 °C			13.1	1.35±0.007	19.1	9.26
γM-PI 350 °C			52.1	1.34±0.01	18.1	-1.60
γM-PI 400 °C			100	1.32±0.029	20.8	8.42
γE-PI	296	309		1.41±0.009	13.7	

γE-PI 300 °C	22.4	1.35±0.013	16.7	6.65
γE-PI 350 °C	100	1.33±0.005	16.5	13.2
γE-PI 400 °C	100	1.27±0.038	20.4	8.29

X-Ray Diffraction Spectroscopy (XRD)

Table S2. Determined d-spacing of Allyl-, αM-, βM-, γM- and γE-PI by means of x-ray diffraction spectroscopy, after annealing at 350 °C for 2 h and 400 °C for 1 h, respectively.

	d-spacing (2°)	
	Annealing temperature (°C)	
Material	**350**	**400**
HPI	0.67	0.60
AllylPI-1	0.53	0.54
αMPI-1		0.55
βMPI-1	0.55	0.59
γMPI-1	0.54	0.51
γEPI-1	0.57	0.53

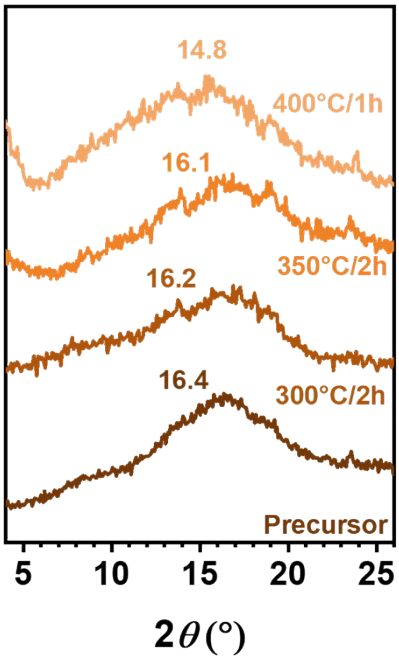

Figure S11. Determined diffraction pattern **of** βMPI-1 by means of x-ray diffraction spectroscopy, after annealing at 350 °C for 2 h and 400 °C for 1 h, respectively

Gas Performance by means of Time-Lag Measurements

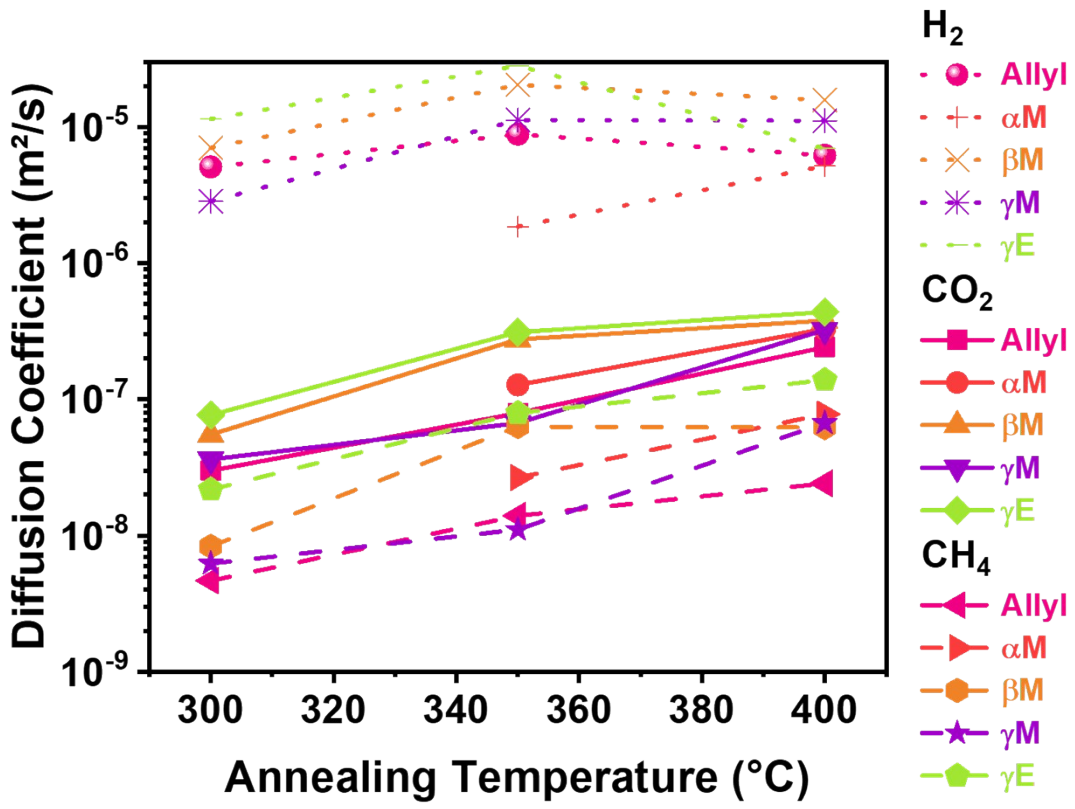

Figure S12. Diffusion coefficient as a function of the annealing temperature for different allyl derivatives for the gases H_2, CO_2 and CH_4.

Table S3. *Overview of determined gas diffusion coefficients of He, H_2, CO_2, O_2, N_2 and CH_4.*

		Diffusion coefficient [10^{-8} cm²/s]					
Material	***Annealing***	***He***	***H2***	***CO2***	***O2***	***N2***	***CH4***
Allyl-PI	***300***	*200*	*509*	*2.99*	*9.42*	*2.44*	*0.47*
βM-PI		*680*	*702*	*5.51*	*16.8*	*3.89*	*0.83*
γM-PI		*554*	*285*	*3.62*	*8.63*	*1.37*	*0.62*
γE-PI		*593*	*1147*	*7.68*	*26.8*	*7.96*	*2.17*
Cinnamyl-PI		*139*	*85.2*	*1.14*	*5.71*	*2.33*	*0.04*

Prenyl-PI		*631*	*458*	*3.03*	*10.5*	*1.01*	*0.35*
Butylene-PI		*196*	*108*	*4.89*	*10.9*	*4.07*	*1.25*
Allyl-PI	***350***	*2638*	*883*	*7.92*	*22.6*	*6.27*	*1.39*
		792	*185*	*12.8*	*31.7*	*10.2*	*2.66*
βM-PI		*3070*	*2050*	*27.5*	*78.5*	*11.2*	*6.30*
γM-PI		*4130*	*1126*	*6.69*	*13.4*	*5.20*	*1.10*
gE-PI		*5431*	*2825*	*31.2*	*75.8*	*29.9*	*7.92*
Cinnamyl-PI		*1217*	*120*	*8.49*	*14.6*	*6.37*	*2.49*
Prenyl-PI			*1110*	*9.74*	*27.9*	*9.31*	*0.45*
Butylene-PI		*1736*	*1471*	*8.19*	*24.1*	*6.65*	*1.18*
Allyl-PI	***400***	*210*	*621*	*24.2*	*25.9*	*5.95*	*2.41*
αM-PI		*491*	*518*	*32.9*	*59.9*	*22.2*	*7.78*
βM-PI		*952*	*1580*	*37.9*	*72.8*	*21.9*	*6.21*
γM-PI		*507*	*1110*	*32.4*	*77.5*	*27.5*	*6.71*
γE-PI		*1850*	*696*	*43.8*	*94.4*	*23.8*	*13.9*
βM-PI	***150***	*41.8*	*188*	*3.35*	*14.3*	*3.32*	*0.52*
	300 1'		*1400*	*4.12*	*7.22*	*2.55*	*0.72*
	300 30'	*680*	*702*	*5.51*	*16.8*	*3.89*	*0.83*
	300 120'	*228*	*1293*	*8.21*	*16.3*	*2.43*	*1.76*
	350	*3070*	*2050*	*27.5*	*78.5*	*11.2*	*6.30*
	400	*952*	*1580*	*37.9*	*72.8*	*21.9*	*6.21*

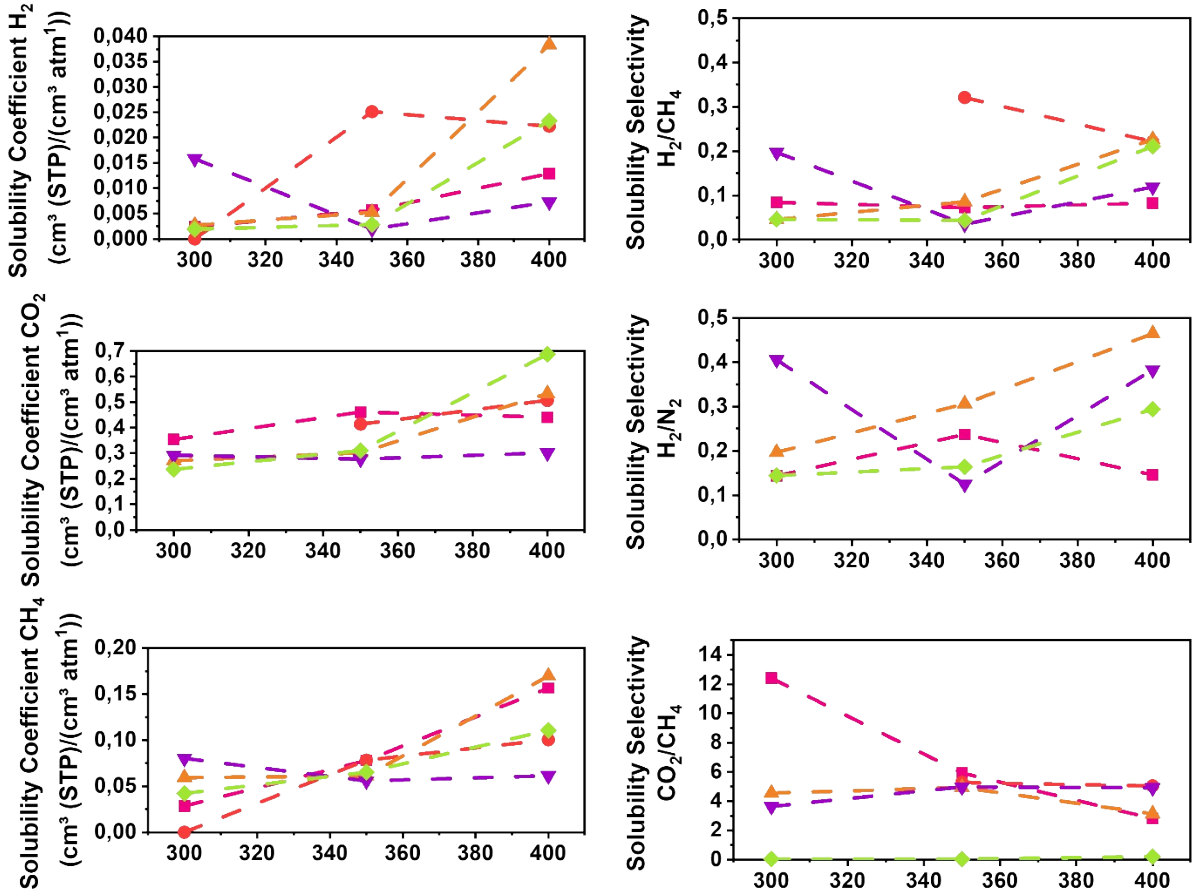

Figure S13. Gas solubility coefficient of He, H_2, CO_2, O_2, N_2 and CH_4 and solubility-based selectivity of the gas pairs H_2/CH_4, H_2/N_2 and CO_2/CH_4 of the studied allylderivatives after annealing at 300 °C for 30 min, 350 °C for 2 h and 400 °C for 1 h.

Table S4. Overview of determined gas solubility coefficients of He, H_2, CO_2, O_2, N_2 and CH_4.

		Solubility coefficient [10^{-3} cm³ (STP) /(cm³ atm¹)]					
Material	**Annealing**	**He**	**H2**	**CO2**	**O2**	**N2**	**CH4**
Allyl-PI	**300**	1,24	2,41	354	19,2	16,7	28,5
βM-PI		2,19	2,72	271	17,4	13,8	59,4
γM-PI		9,64	15,8	292	28,8	39,1	80,3
γE-PI		3,06	1,93	237	13,6	13,4	42,2
Cinnamyl-PI		0,001	0,0008	240	18,0	16,4	902
Prenyl-PI		2,46	3,09	279	17,7	41,0	105
Butylene-PI		9,07	12,9	245	23,9	22,5	51,2
Allyl-PI	**350**	1,61	5,66	461	26,0	23,8	77,9
αM-PI		9,18	25,1	413	31,8	26,2	78,3
βM-PI		2,38	5,26	302	21,6	17,1	61,2
γM-PI		0,49	1,95	277	16,9	15,6	55,7
γE-PI		0,99	2,84	3111	21,4	17,3	65,2
Cinnamyl-PI		0,001	0,001	293	38,0	35,9	78,4
Prenyl-PI		0,09	2,66	243	18,3	14,1	26,2
Butylene-PI		1,95	1,97	275	20,2	17,5	64,6
Allyl-PI	**400**	29,2	12,9	441	72,9	88,4	157
αM-PI		15,3	22,3	507	48,6	39,9	101
βM-PI		9,9	38,4	533	85,4	82,6	170
γM-PI		11,3	7,32	302	22,1	19,1	61,4
γE-PI		4,93	23,3	682	55,8	79,4	111
βM-PI	**150**	14,0	2,17	94,3	4,09	12,6	23,9

	300 1'	-	8,72	267	25,8	19,2	46,3
	300 30'	2,19	2,72	271	17,4	13,8	59,4
	350	2,38	5,26	302	21,6	17,1	61,2
	400	9,9	38,4	533	85,4	82,6	170

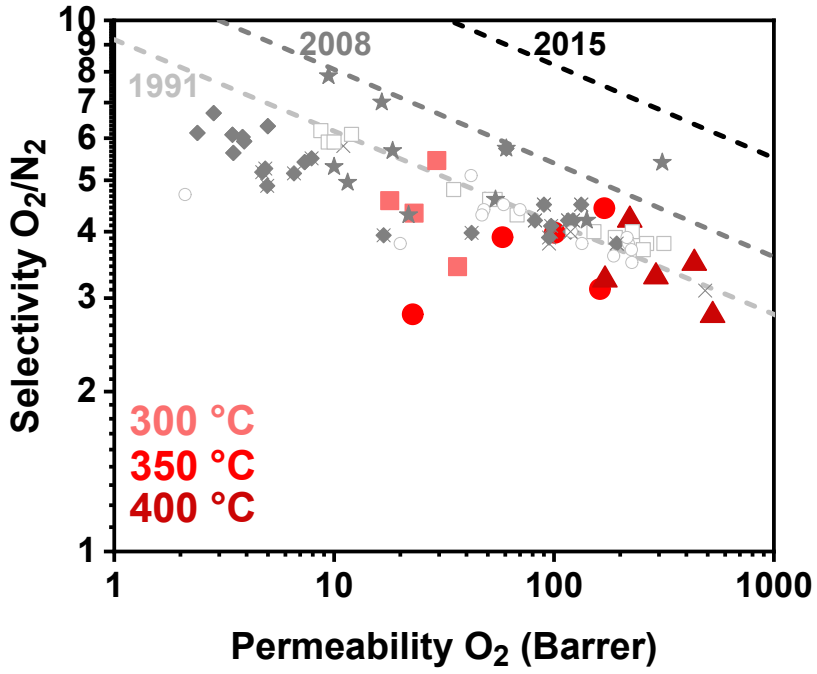

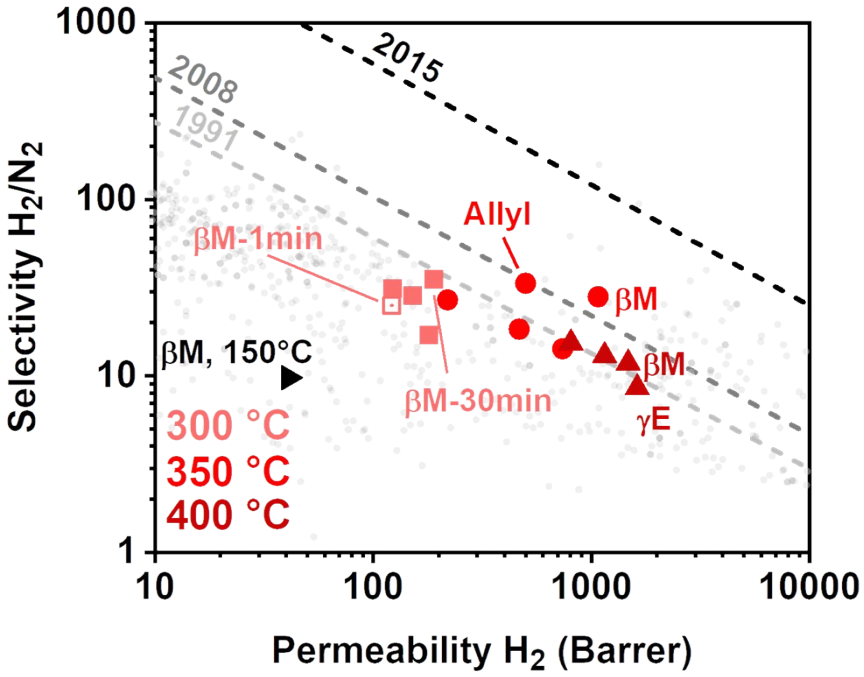

Figure S14. Gas pair selectivity vs gas permeability of O_2/N_2 for different allylderivatives after annealing at 300 °C for 0.5 h (■), 350 °C for 2 h (●) and 400 °C for 1 h (▲), incorporated in the upper bound plot, including upper bounds of 1991, 2008 and 2015 [4].

Table S5. Overview of determined gas permeability of He, H_2, CO_2, O_2, N_2 and CH_4.

		Permeability [Barrer]					
Material	**Annealing**	**He**	**H2**	**CO2**	**O2**	**N2**	**CH4**
Allyl-PI	**300**	247	122	102	17.9	3.91	1.39
βM-PI		180	189	149	29.3	5.38	4.94
γM-PI		151	152	106	23.1	5.33	4.99
γE-PI		167	180	181	36.5	10.6	9.16
Cinnamyl-PI		95.8	99.8	50.6	10.3	3.81	3.59
Prenyl-PI		155	141	84.5	18.5	4.13	3.63
Butylene-PI		142	140	120	25.8	9.08	6.41
Allyl-PI	**350**	423	499	377	58.3	14.9	10.9
αM-PI		727	467	527	101	25.4	20.8
βM-PI		728	1075	831	169	38.3	38.2
γM-PI		204	219	185	22.8	8.15	6.14
γE-PI		531	739	968	162	51.9	51.6
Cinnamyl-PI		226	269	249	55.1	22.8	19.2
Prenyl-PI		271	295	236	50.9	13.1	11.7
Butylene-PI		287	289	225	48.5	11.6	7.19
Allyl-PI	**400**	613	803	1066	221	52.6	37.8
aM-PI		752	1151	1669	291	88.3	78.2
βM-PI		944	1475	1984	434	125	93.1
γM-PI		575	808	975	171	52.5	41.2
γE-PI		913	1624	3011	526	189	153
βM-PI	**150**	58.7	40.9	63.1	11.8	4.19	2.48
	300		122	110	18.6	4.86	3.23
	300	180	189	149	29.3	5.38	4.94
	350	728	1075	831	169	38.3	38.2
	400	944	1475	1984	434	125	93.1

Table S6. Overview of determined gas selectivity certain gas pairs.

		Selectivity					
Material	**Annealing**	**H2/CO2**	**H2/N2**	**H2/CH4**	**O2/N2**	**CO2/CH4**	**CO2/N2**
Allyl-PI	**300**	1.20	31.3	88.2	4.6	51	26.1
βM-PI		1.27	35.2	38.4	5.4	30.2	27.7
γM-PI		1.44	28.5	30.5	4.3	21.2	19.9
γE-PI		0.99	16.9	19.7	3.4	19.8	17.1
Cinnamyl-PI		1.97	26.2	27.8	2.7	14.1	13.3
Prenyl-PI		1.68	34.2	38.9	4.5	23.3	20.5
Butylene-PI		1.17	15.4	21.8	2.8	18.6	13.2
Allyl-PI	**350**	1.32	33.4	45.9	3.9	34.7	25.3
αM-PI		0.89	18.4	22.4	4.0	25.3	20.8
βM-PI		1.29	28.1	28.2	4.4	21.8	21.7
γM-PI		1.18	26.9	35.7	2.8	30.2	22.7
γE-PI		0.76	14.2	14.3	3.1	18.8	18.7
Cinnamyl-PI		1.08	11.8	13.8	2.4	12.8	10.9
Prenyl-PI		1.25	22.6	25.3	3.9	20.2	18.1
Butylene-PI		1.29	24.9	40.2	4.2	31.3	19.4
Allyl-PI	**400**	0.75	15.3	21.2	4.2	28.2	20.3
αM-PI		0.69	13.0	14.7	3.3	21.3	18.9
βM-PI		0.74	11.8	15.8	3.5	21.3	15.9
γM-PI		0.83	15.4	19.6	3.2	23.7	18.6
γE-PI		0.54	8.6	10.6	2.8	19.6	15.9
βM-PI	**150**	0.65	9.8	16.5	2.8	25.5	15.0
	300	1.10	25.0	37.7	3.8	34.0	22.7
	300	1.27	35.2	38.4	5.4	30.2	27.7
	350	1.29	28.1	28.2	4.4	21.8	21.7
	400	0.74	11.8	15.8	3.5	21.3	15.9

Table S7. Overview of determined gas diffusion coefficients of ethylene, ethane, propylene and propane.

Diffusion coefficient [10^{-8} cm²/s]					
Material	**Annealing**	**C2H4**	**C2H6**	**C3H6**	**C3H8**
Allyl-PI	**400**	1.18	0.35	0.21	0.019
αM-PI		2.11	0.72	0.46	0.049
βM-PI		4.00	1.28	0.98	0.06
γE-PI		3.8	1.19	0.74	0.057

Table S8. Overview of determined gas solubility coefficients of ethylene, ethane, propylene and propane.

Solubility coefficient [10^{-3} cm³ (STP) /(cm³ atm^{1})]					
Material	**Annealing**	**C2H4**	**C2H6**	**C3H6**	**C3H8**
Allyl-PI	**400**	524	741	1694	1493
αM-PI		660	817	1650	1246
βM-PI		593	879	1257	1019
γE-PI		859	1271	2794	2617

Table S9. Overview of determined gas permeability of ethylene, ethane, propylene and propane.

Permeability [Barrer]					
Material	**Annealing**	**C2H4**	**C2H6**	**C3H6**	**C3H8**
Allyl-PI	**400**	61.5	25.5	35.5	2.88
αM-PI		139	59.0	76.0	6.15
βM-PI		237	113	123	6.16
γE-PI		327	151	207	14.9

Table S10. Overview of determined gas selectivity certain gas pairs.

Selectivity			
Material	**Annealing**	**C2H4/ C2H6**	**C3H6/ C3H8**
Allyl-PI	**400**	2.4	12.3
αM-PI		2.4	12.4
βM-PI		2.1	19.9
γE-PI		2.2	13.9

Computational Chemistry

Quantum mechanical Simulation

Geometry optimized Structures

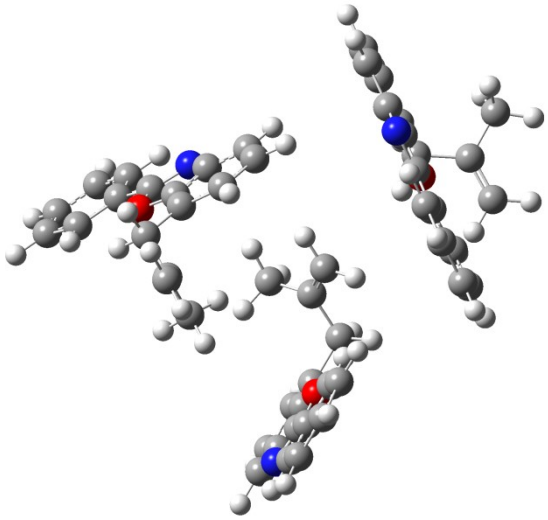

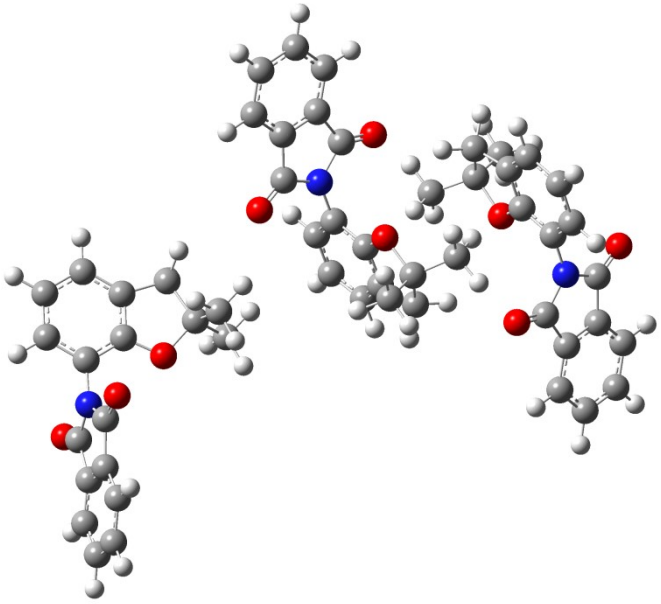

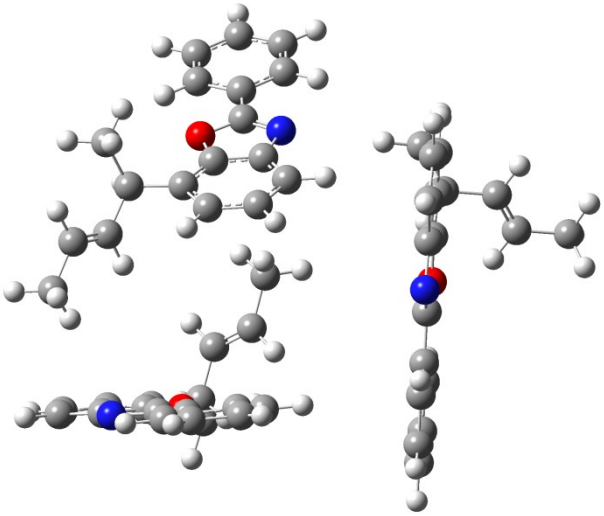

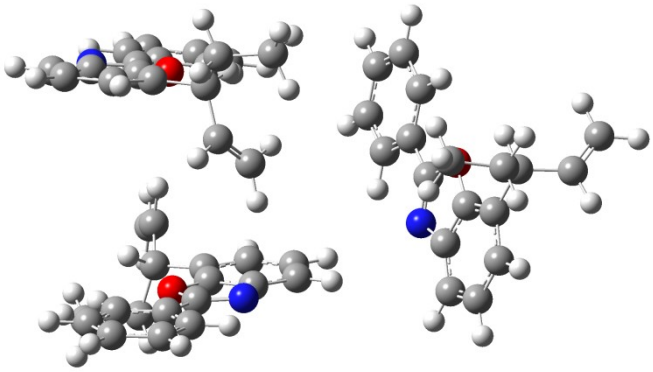

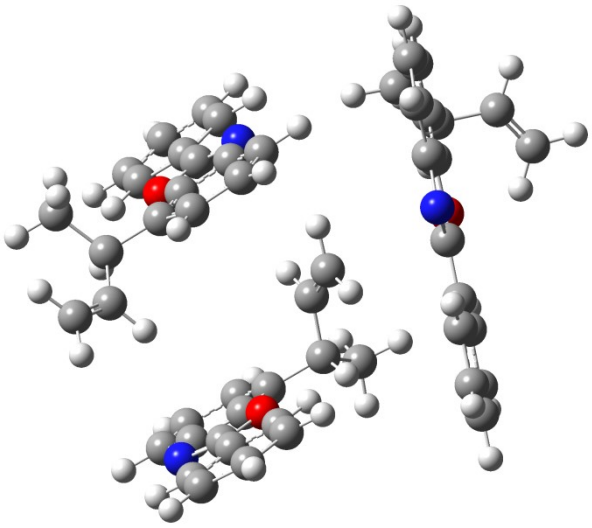

Figure S15. Geometry optimized structures of three models of each allylderivative.

Potentialenergy surface scan

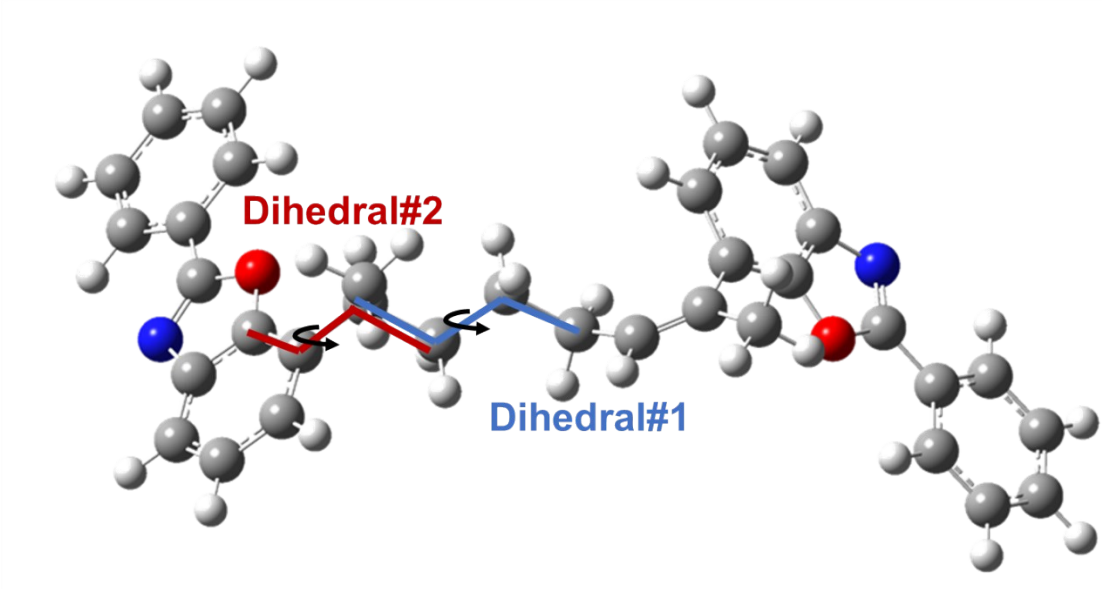

Figure S16. Visulaization of the investigated dihedral angle of the studied allylderivatives.

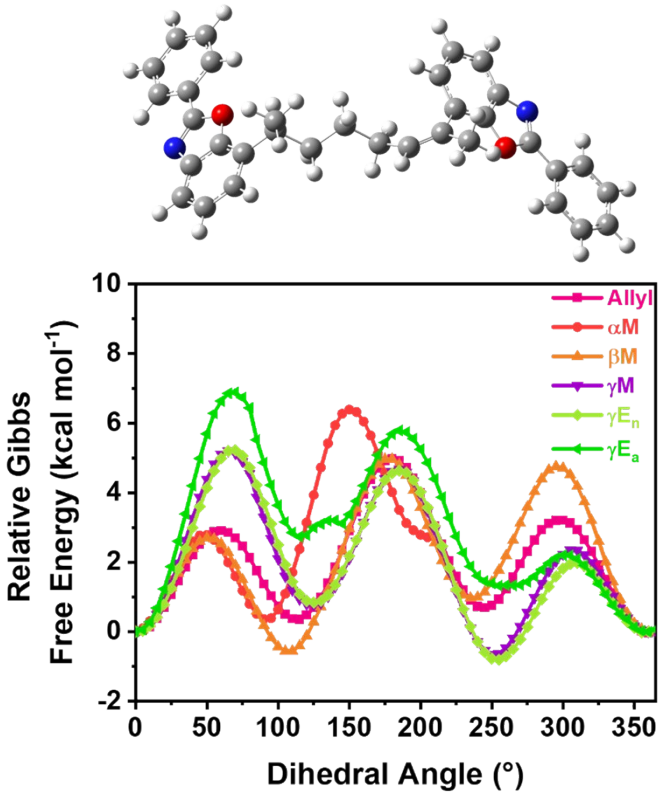

Figure S17. PES scan of the dihedral angle (red mark up) of Allyl-PBO (left), PES scan of the dihedral angle of allylderivatives βM-PBO, γM-PBO, γEn-PBO and γEa-PBO.

Molecular Modelling

Method

The polymer models were built from previously constructed and optimized single repetition units. The prepared polymer models were also optimized by an energy minimization step.

From these optimized polymer models several amorphous cells were constructing, following the Theodorou/Suter method, which is implemented in the Amorphous Cell module of Materials Studio. Every cell was constructed from two polymer chains, each containing 40 repetition units, with a total of 6564 atoms (in the case of γM-PI) at an initial density of 0.1 g cm^{-3} at 303 K under periodic boundary conditions. The final packing of the cell at the final density was obtained after a compression-decompression procedure (Table S8) [5]. This relaxation and equilibration method is described more in detail in the support information. A long final NpT-MD runs was carried out to equilibrate the model. A validity check was done by varifying a stable energy and density after long MD runs. In order to check the quality of the boxes the ratio of the accessible volume (AV) to accessible solvent surface (ASA) and its gradient by varying the probe radius from 1.0 to 2.0 A with steps of 0.1 A was done [6, 7]. The final cell size of the packing models was about $(40A)^3$

Table S11. Overview of the compression-decompression-relaxations procedure to generate amorphous cells.

Step#	Temperature (K)	Pressure (GPa)	Time (ps)	Ensemble
1	600		50	NVT
2	303		50	NVT
3	303	0.003	50	NPT
4	600		50	NVT
5	303		100	NVT

6	303	0.05	50	NPT
7	600		50	NVT
8	303		100	NVT
9	303	0.3	50	NPT
10	600		50	NVT
11	303		100	NVT
12	303	0.15	5	NPT
13	600		5	NVT
14	303		10	NVT
15	303	0.06	5	NPT
16	600		5	NVT
17	303		10	NVT
18	303	0.0001	5	NPT
19	600		5	NVT
20	303		10	NVT
21	303	0.0001	300	NPT
Final	303		500	NVT

The subsequent crosslinking procedure was developed by a set of crosslinking reactions between corresponding allylgroups followed by an geometry optimization and a 30ps NPT and 30ps NVT MD-run. The procedure was repeated until no crosslinking allyl groups were found within the pre-specified cut-off distance of 5A. The scheme is demonstrated in the support information.

The analysis of the structure properties, such as the torsional distribution, length distribution of certain subunits, as well as the means-square displacement (MSD) was done by means of long 1ns-MD runs with a NVT-ensemble at 600 K and 303K with a time-step of 1 femtosecond. The temperature control was performed by using a Nosé thermostat.

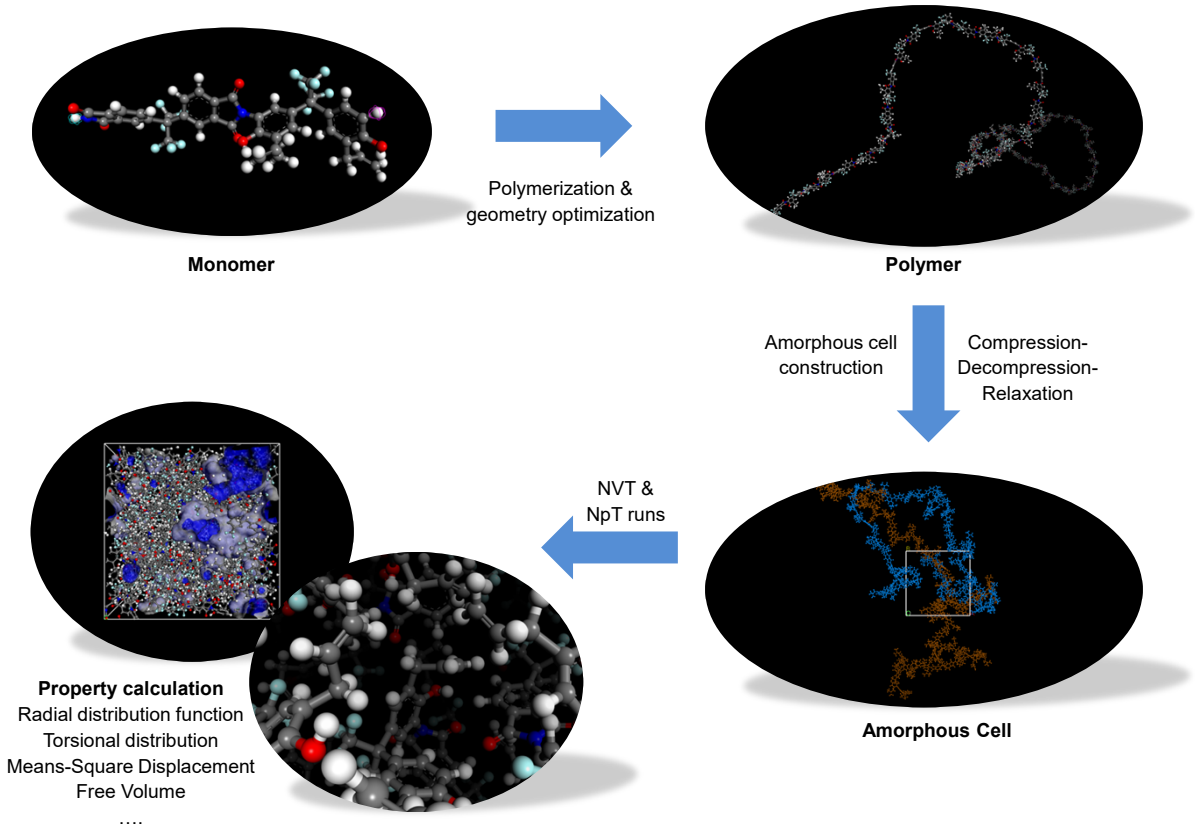

Scheme S3: Amorphous cell development procedure including (1) monomer creation and optimization, (2) polymer building, (3) amorphous cell packing followed by a 21step procedure including compression-decompression-relaxation and equilibration runs, (4) analytics via long NVT or NpT-runs.

The free volume analysis was perfomed using the visualizer tool of materials studio. The free accessible volume (FAV), defined by the cell volume V and the probe accessible volume Vprobe, was determined by the ratio as show in equation

$$FAV\ (\%) = \frac{V - V_{Probe}}{V} x100$$

Table S12. Overview of determined parameter and properties obtained by molecular modelling simulations.

Code	Atom#	Crosslinks	Density
Allyl	4624	0	1.354±0.005
Allyl10cx	4624	10	1.362±0.012
Allyl20cx	4624	20	1.351±0.009
Allyl33cx	4624	33	1.361±0.014
αM-PI	5020	0	1.356±0.007
αM-PI10cx	5020	10	1.343±0.001
αM-PI20cx	5020	20	1.337±0.009
αM-PI27cx	5020	27	1.331±0.001
βM-PI	5020	0	1.358±0.005
βM-PI10cx	5020	10	1.322±0.024
βM-PI20cx	5020	20	1.331±0.012
βM-PI26cx	5020	26	1.335±0.014
PBF- βM-PI	5020	0	1.349±0.003
γM-PI	5020	0	1.347±0.001
γM-PI10cx	5020	10	1.319±0.000
γM-PI20cx	5020	20	1.320±0.001
γM-PI29cx	5020	29	1.308±0.000
γE-PI	5416	0	1.349±0.004
γE-PI10cx	5416	10	1.258±0.041
γE-PI20cx	5416	20	1.289±0.019
γE-PI26cx	5416	26	1.302±0.013
γEa-PI	5416	0	1.345±0.008
γEa-PI10cx	5416	10	1.288±0.012

γEa-PI20cx	5416	20	1.301±0.005
γEa-PI21cx	5416	21	1.252±0.050

Table S13. Overview of free volume analysis of βM-PI.

Code	Crosslinks	Density	Free Volume (%)	Free Volume/ Connolly Surface (Å)
βM-PI	0	1.358±0.005	23.58±0.36	0.76±0.019
βM-PI10cx	10	1.322±0.024	25.73±1.82	0.88±0.006
βM-PI20cx	20	1.331±0.012	25.85±2.38	0.87±0.031
βM-PI26cx	26±1	1.335±0.014	25.62±1.83	0.84±0.0006
CyCx-βM-PI	26±1	1.331 ± 0.011	26.58±0.006	0.83±0.014
(TCM)βM-PI	26±1	1.313±0.016	26.77±0.010	0.81±0.04
(TCM)βM-PI	26±1	1.298 ± 0.013	27.44±0.009	0.81±0.027
(TCM)βM-PI	26±1	1.270±0.007	28.14±0.006	0.83±0.023
PBF- βM-PI	0	1.349±0.003	25.63±0.295	0.79±0.021

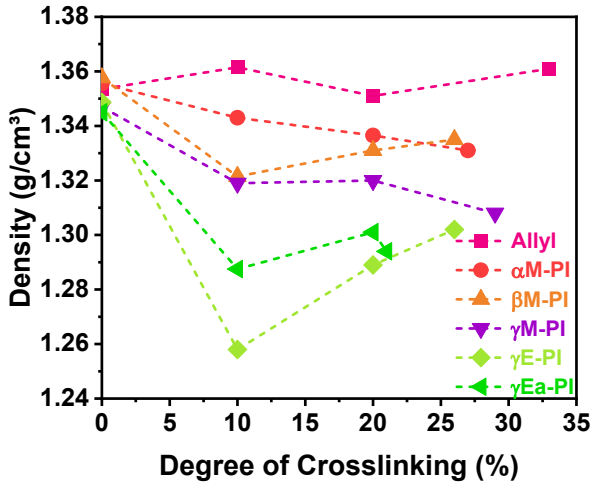

Figure S18. Free volume elements with an increasing number of crosslinks and a depiction of the density as a function of the degree of crosslinking of all allyl derivatives (left).

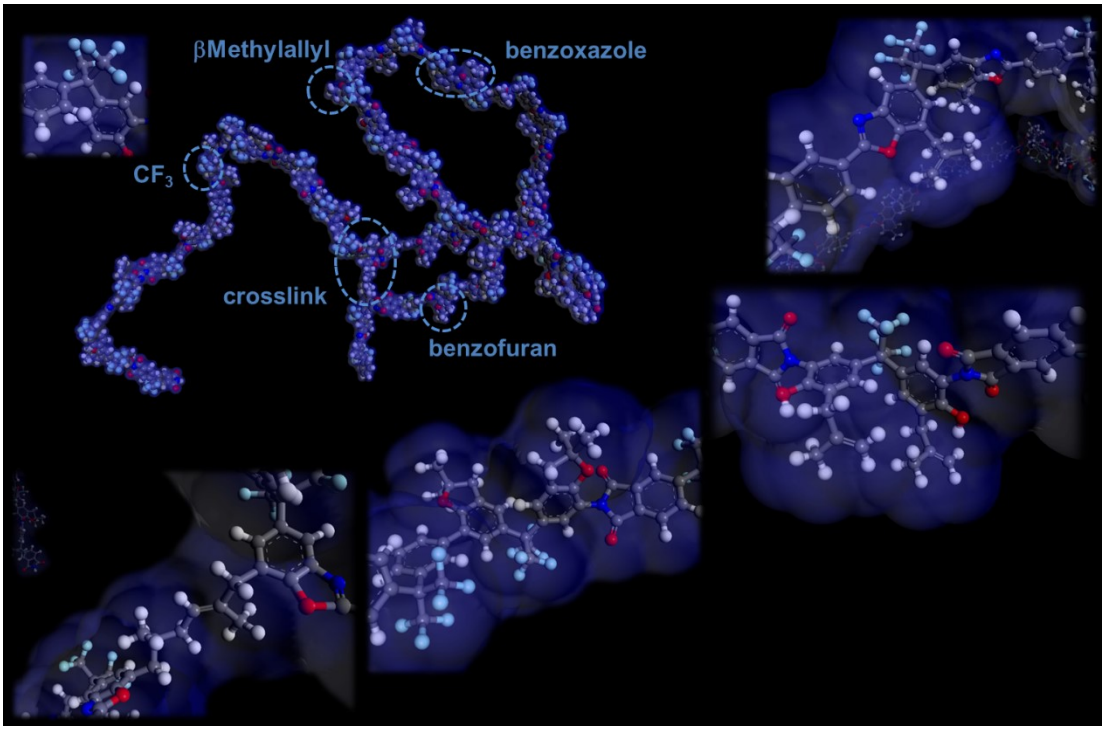

Figure S19. βM-PI polymer chain containing benzofuran, Claisen-Rearranged, crosslinked and thermally rearranged units.

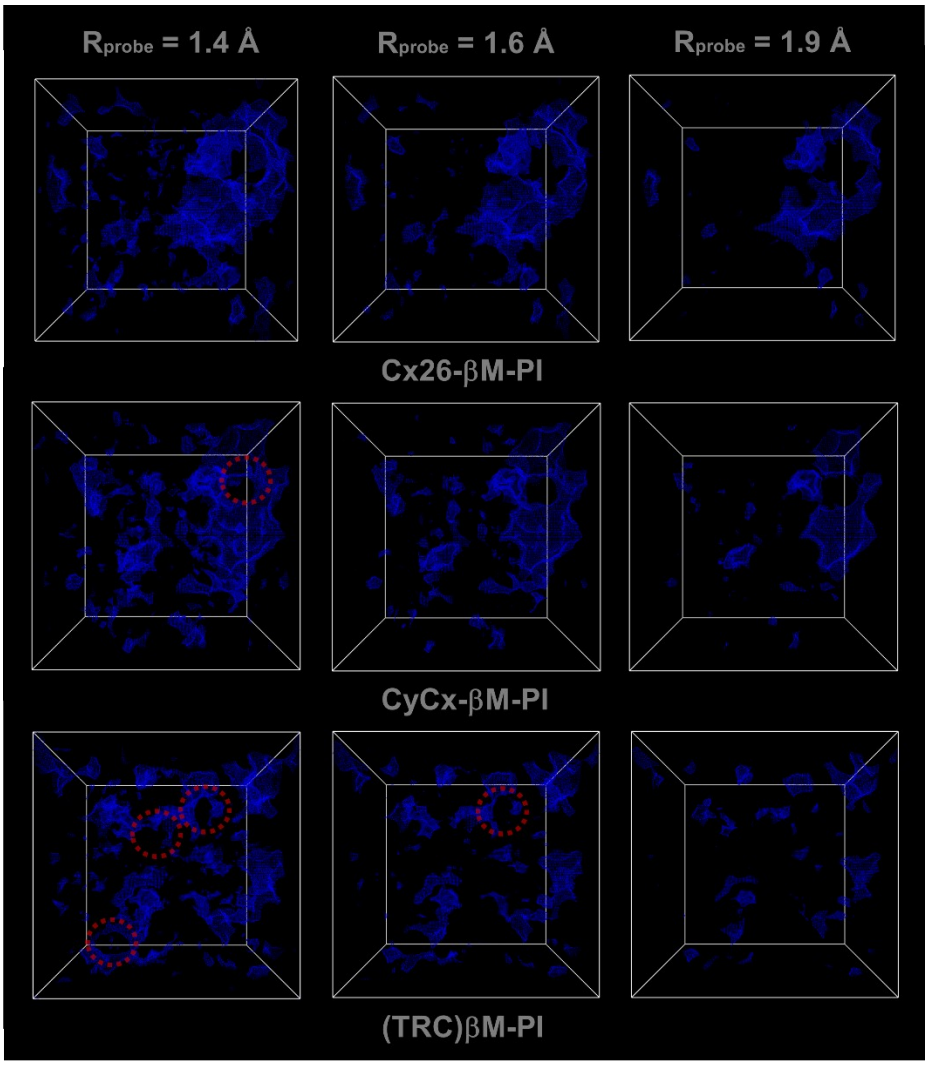

Figure S20. Accessible free volume at a probe radius of 1.4 Å (left), 1.6 Å (middle) and 1.9 Å (right) is shown for CyCx-βM-PI (top row) and (TRC)βM-PI (bottom row).

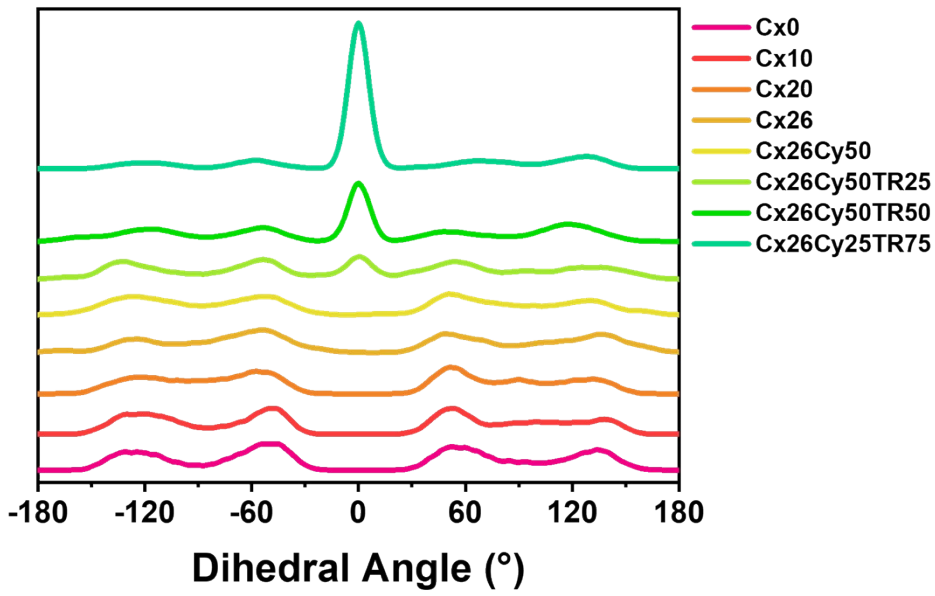

Figure S21. Torsion distribution for the imide-phenol dihedral torsion with increasing degree of crosslinking (0-26) and CyCx-βM-PI, (TCR)βM-PI with 25, 50 and 75% HPI-to-PBO conversion.

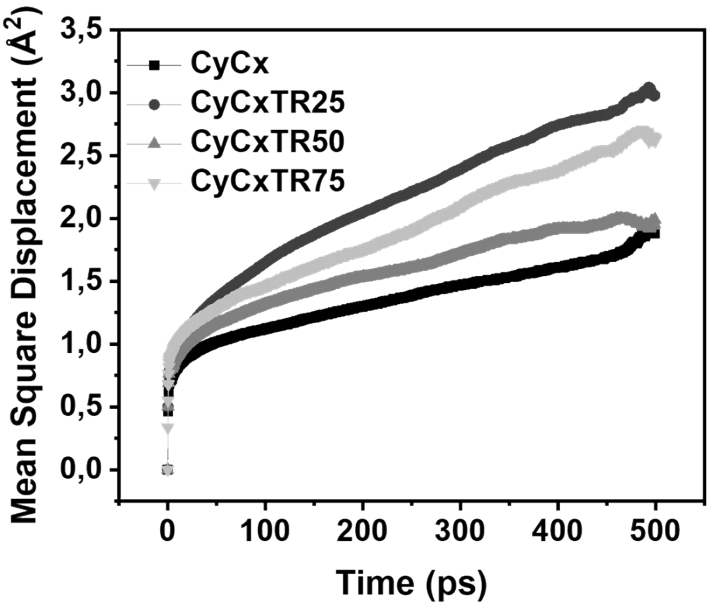

Figure S22. Mean-Square Displacement for CyCx-βM-PI, (TCR)βM-PI with 25, 50 and 75% of HPI-to-PBO conversion.

References

1. Bondi, A., *van der Waals Volumes and Radii.* The Journal of Physical Chemistry, 1964. **68**(3): p. 441-451.
2. Park, J.Y. and D.R. Paul, *Correlation and prediction of gas permeability in glassy polymer membrane materials via a modified free volume based group contribution method.* Journal of Membrane Science, 1997. **125**(1): p. 23-39.
3. Shishatskii, A.M., Y.P. Yampol'skii, and K.V. Peinemann, *Effects of film thickness on density and gas permeation parameters of glassy polymers.* Journal of Membrane Science, 1996. **112**(2): p. 275-285.
4. Swaidan, R., B. Ghanem, and I. Pinnau, *Fine-Tuned Intrinsically Ultramicroporous Polymers Redefine the Permeability/Selectivity Upper Bounds of Membrane-Based Air and Hydrogen Separations.* ACS Macro Letters, 2015. **4**(9): p. 947-951.
5. Larsen, G.S., et al., *Molecular Simulations of PIM-1-like Polymers of Intrinsic Microporosity.* Macromolecules, 2011. **44**(17): p. 6944-6951.
6. Park, C.H., et al., *A simulation study on OH-containing polyimide (HPI) and thermally rearranged polybenzoxazoles (TR-PBO): relationship between gas transport properties and free volume morphology.* J Phys Chem B, 2014. **118**(10): p. 2746-57.
7. Park, C.H., et al., *Thermal treatment effect on the structure and property change between hydroxy-containing polyimides (HPIs) and thermally rearranged polybenzoxazole (TR-PBO).* J Phys Chem B, 2012. **116**(42): p. 12864-77.